Crack growth in non-homogeneous transformable ceramics. Part I

Stam, Geert; Giessen, Erik van der

Published in:
International Journal of Fracture

DOI:
10.1007/BF00019380

International Journal of Fracture **79:** 249–271, 1996.

Crack growth in non-homogeneous transformable ceramics. Part I: Constrained straight cracks

GEERT STAM* and ERIK VAN DER GIESSEN
Delft University of Technology, Laboratory for Engineering Mechanics, Delft, The Netherlands

Received 10 May 1995; accepted 8 March 1996

Abstract. Crack growth in transformable ceramics is studied using a finite element approach. In the analysis, a continuum theory is used for the description of the inelastic deformation due to a stress-induced martensitic type phase transformation with both dilatation and shear strain components. Attention is focussed on materials in which the transformable phase is not distributed homogeneously, as is the case in, for example, most ZTA materials and Duplex Ceramics. In this paper, the distribution of transformable phase is assumed to be symmetric with respect to the crack plane; in the companion paper [1] this assumption is left. The effect of the heterogeneity on the toughness is studied in detail. A small scale boundary value crack problem is formulated and an incremental loading algorithm with a nodal release technique is used to simulate crack advance. It is found that in all cases studied the maximum toughness improved relative to homogeneous materials with the same average volume fraction of zirconia. The results are presented in plots of transformation zones and crack-growth resistance curves.

1. General introduction

The fact that the stress-induced transformation in tetragonal zirconia can improve the toughness considerably has been known since the mid seventies (see e.g. Evans and Heuer [2]). Many transformation toughened materials have been developed since; for an overview see, for instance, Green et al. [3]. In this paper we will study the crack-growth behavior of two of these materials: Zirconia Toughened Alumina (ZTA) and Duplex materials. ZTA materials are composites and consist of a non-transformable alumina (Al_2O_3) matrix containing transformable tetragonal zirconia (t-ZrO_2) grains [4]. In most materials, about 30 percent of the composite is zirconia and the zirconia grain size is of the order of 1 μm. Usually the alumina grains are slightly larger. In Duplex materials the matrix also consists of alumina, but instead of being dispersed in the matrix, the zirconia is clustered in spherical inclusions with diameters ranging from 10 to 50 μm [5].

Two stress-induced zone-shielding toughening mechanisms are believed to play a role in these materials. Namely, transformation toughening and microcrack toughening, as indicated by, among others, Rühle et al. [4] for ZTA, and Lutz and Claussen [5] for Duplex Ceramics. The first toughening mechanism relies on the martensitic-type of crystal transformation in zirconia where tetragonal material (t) transforms into a monoclinic structure (m). The transformation takes place at a critical stress level, and in an unconstrained crystal the transformation yields a volume expansion of about 4.5 percent and a shear component of about 16 percent. However, if the inclusion is constrained by the matrix, twinning can reduce the shear component considerably [6]. In the high-stress field around the crack tip the transformation occurs first and the transformation strains can shield the tip from the applied stresses. The second, microcrack toughening mechanism relies on the residual stresses around already transformed

* Currently at Rutgers University, College of Engineering, Department of Ceramics, Piscataway, NJ, USA

monoclinic-zirconia inclusions. In the neighbourhood of the crack tip, these stresses can cause the inclusion to separate from the matrix, and microcracks are introduced in the composite. These microcracks can also shield the tip from the applied stresses [7].

Throughout this and the accompanying work [1], we assume that the transformation toughening mechanism completely dominates the microcrack mechanism. In our model the transformable inclusions stay coherently embedded in the linear elastic non-transformable matrix. Also, toughening by other mechanisms, such as contact shielding (wedging caused by broken-out grains or rough crack surfaces and crack bridging), and crack deflection or branching, is not accounted for. In the companion paper [1], we study the effect of crack deflection due to transformation strains.

In this work we will study the effect of a non-homogeneous distribution of transformable inclusions on the crack-growth behaviour. The subject emerged from findings of Den Exter [8], who studied ZTA materials which were prepared from fine-grained zirconia and alumina powders. He tried to obtain ZTA materials with small t-zirconia grains to improve the mechanical properties, particularly the toughness. It was found that during processing of this composite, prior to sintering, the fine-grained powders tended to agglomerate, which during the sintering process caused a non-homogeneous distribution of zirconia in the alumina matrix. A great deal of effort had been put into the development of composites with a homogeneous distribution, but the question was raised whether a certain level of heterogeneity would, or perhaps would *not*, decrease the toughness of the material. Here, we consider this problem using a continuum model developed by Sun et al. [9]. This model accounts for both the dilatant and shear-strain components of the transformation. It is therefore more realistic than an earlier model [10, 11] which only took into account the dilatant part of the transformation strain, assuming twinning would relax all transformation shear strains. This assumption was proven to be incorrect by, among others, Chen and Reyes–Morel [12, 13], who have performed hydraulic compression tests that showed shear and dilatation effects of comparable magnitude. Results of crack-growth studies with the afore-mentioned model for materials with a homogeneously distributed transformable phase (Partially Stabilized Zirconia (PSZ) and Tetragonal Zirconia Polycrystal (TZP) materials) have been presented in [14] and [15]. To allow comparison with these previous results, we also performed crack-growth simulations with the transformation being solely dilatant. Preliminary results for non-homogeneously distributed transformable phase and dilatant transformation behavior were published in [16].

Standard tensor notation is used, with tensors being denoted with bold-face characters. Cartesian components with indices running from 1 to 3 are indicated with Latin subscripts, while Greek subscripts run from 1 to 2 only. The second-order unit tensor is $\boldsymbol{I}$, and tr denotes the trace. The tensor product is denoted by $\otimes$ and the following operations apply to any fourth-order tensor $\boldsymbol{L}$ and second order tensors $\boldsymbol{A}$ and $\boldsymbol{B}$ ($\boldsymbol{e}_i$ are Cartesian base vectors): $\boldsymbol{LA} = L_{ijkl}A_{kl}(\boldsymbol{e}_i \otimes \boldsymbol{e}_j), \boldsymbol{A} \cdot \boldsymbol{B} = A_{ij}B_{ij}$. A superposed dot denotes the time derivative; since we will not be concerned with true time dependent phenomena, any monotonically increasing parameter may serve as a 'time' parameter. The crack analysis will be carried out with plane strain conditions.

2. Problem formulation

2.1. DISTRIBUTION OF TRANSFORMABLE PHASE

Figure 1 shows the schematic microstructure of a ZTA material. In fact, the figure is a composition of 6 schematic representations of the same micrograph made by Rühle et al. [17]. The zirconia particles are shown as dark. It is clear that the zirconia particles are not distributed homogeneously and that areas with high and low content of zirconia can be found. On the right-hand side of the figure an experimentally derived percentage of transformed zirconia phase is given. This may be interpreted as the profile of the transformation zone perpendicular to the crack surface. This profile is inserted to be able to compare the typical length scale of the clusters to the size of the transformation zone. The heterogeneous distribution of the zirconia phase is analyzed using a 'smeared out' approach. We assume that areas with a higher density of tetragonal phase are separated by areas with a lower density of transformable phase according to a doubly-periodic pattern. The non-homogeneous distribution is represented here by a function $D(X_1, X_2)$, such that the locally available transformable phase f^m is no longer constant over the area, but varies periodically according to

$$f_D^m(X_1, X_2) \equiv D(X_1, X_2) f^m, \tag{1}$$

with $D(X_1, X_2)$ a non-dimensional periodic function defined by

$$D(X_1, X_2) \equiv 1 + C_A \cos\left(\frac{2\pi X_1}{L_c}\right) \cos\left(\frac{2\pi X_2}{L_c}\right) \quad \text{with } C_A \in [0, 1]. \tag{2}$$

The amplitude C_A is the relative deviation from the average value f^m and the characteristic length L_c represents the characteristic period of the heterogeneity. Note that the average amount of transformable phase in a unit volume remains constant. The two periodic functions at the sides of the micrograph in Figure 1 indicate the wave length of the variations in (1). Once the parameters C_A and L_c are chosen, the periodic distribution of available transformable phase $f_D^m(X_1, X_2)$ is defined, as illustrated in Figure 2.

To represent the relatively large inclusions in a Duplex material, the same distribution function (2) is used. However, now $f_D^m(X_1, X_2)$ is a step function, which has zero value in the matrix and unit value in the transformable inclusion. In this paper, we focus on a single particular volume fraction of inclusions, specified by taking a cut-off value of 1.5 for $D(X_1, X_2)$ (with $C_A = 1$), i.e.

$$f_D^m(X_1, X_2) \equiv \begin{cases} 0 & \text{if} \quad (D(X_1, X_2) \leqslant 1.5) \\ 1 & \text{if} \quad (D(X_1, X_2) > 1.5) \end{cases} \quad \text{with } C_A = 1. \tag{3}$$

With this distribution and size of transformable spots it follows that the fraction of transformable phase $f^m = 0.185$ per unit volume. Note that in this case, each zirconia cluster is represented individually, whereas in the above case of ZTA materials only the density of transformable material is varied.

The (X_1, X_2)-coordinate system in the distribution function can be set independently from the (x_1, x_2)-system that will be used to describe the crack-tip fields. The origin of the latter coincides with the initial crack-tip position. In the present Part I of this study, we limit attention to problems in which the transformable phase is distributed symmetrically with respect to the

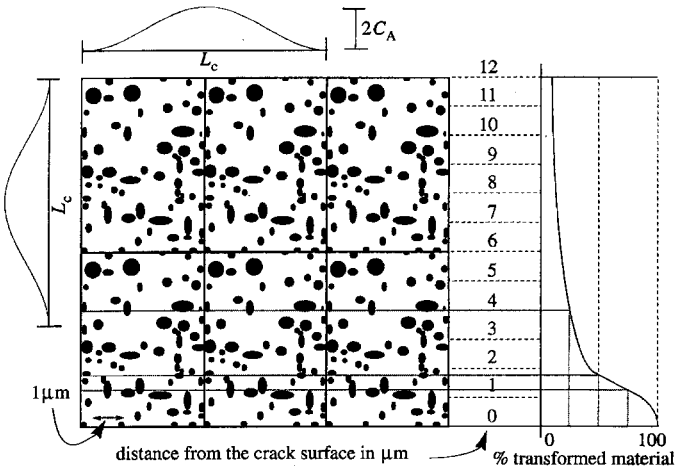

Figure 1. Schematic representation of the microstructure of a ZTA material, where the zirconia particles appear dark. The distribution of transformed material perpendicular to the crack surface has been plotted on the right-hand side.

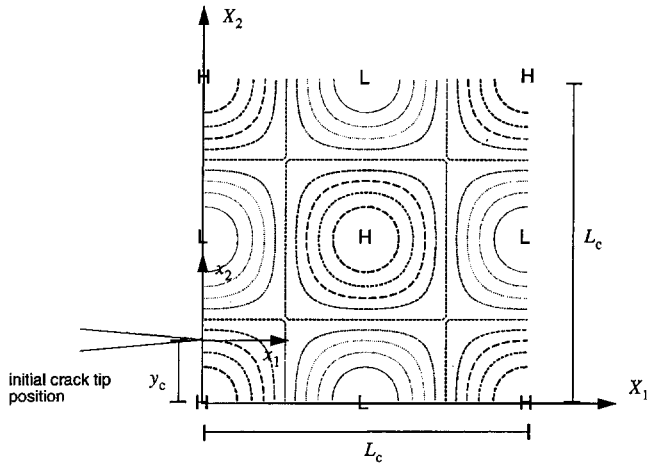

Figure 2. Assumed periodic distribution of transformable phase, were L corresponds with a transformable phase of $(1 - C_A)f^m$ and H to $(1 + C_A)f^m$.

crack plane $x_2 = 0$. When the loading respects the same symmetry, the crack will propagate along $x_2 = 0$. With the distribution function $D(X_1, X_2)$ as in (2), three orientations are possible which maintain symmetry, but here we concentrate on the case where the (X_1, X_2) and(x_1, x_2)-coordinate systems coincide. Results for other paths have been described in [22]. In Part II [1], the (X_1, X_2) and (x_1, x_2)-coordinate systems are chosen to be parallel, but with an offset y_c perpendicular to the initial crack (see Figure 2). Hence, symmetry is lost and the crack will not remain straight [1].

2.2. SMALL SCALE TRANSFORMATION PROBLEM

Experiments [18] have shown that the height of the transformation zone h is small compared to the crack length a. If this condition is met the stress field remote from the tip is not disturbed

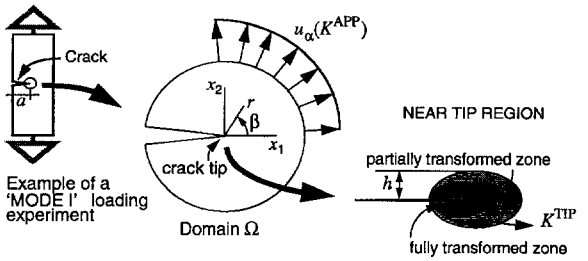

Figure 3. The small-scale transformation assumption and the corresponding boundary value problem for a semi-infinite crack subjected to mode I loading.

by the transformation strains and an asymptotic problem can be formulated for a semi-infinite crack (see Figure 3). This is a so-called small scale transformation problem in which the stress field, $\Sigma_{ij}(r, \beta)$, remote from the tip is given by

$$\Sigma_{ij} = \frac{K^{\text{APP}}}{\sqrt{2\pi r}} f_{ij}(\beta), \quad (r \to \infty) \tag{4}$$

in terms of the elastic stress intensity factor K^{APP} (which will be referred to as the applied stress intensity factor) and the well-known angular functions $f_{ij}(\beta)$. Here, r and β are the radial and angular coordinate measured from the current position of the crack tip, which initially is at $x_1 = x_2 = 0$. As the tip is approached, the transformation zone is encountered (see Figure 3), and the remote stress-field is disturbed by the transformation strains. In the immediate vicinity of the crack tip, the material will be fully transformed, so that its incremental response is again elastic. Inside the fully-transformed zone, a similar crack-tip stress field as in (4) can be found, but with a different stress intensity factor K^{TIP}

$$\Sigma_{ij} = \frac{K^{\text{TIP}}}{\sqrt{2\pi r}} f_{ij}(\theta), \quad (r \to 0). \tag{5}$$

It is assumed that the stress intensity factor at the tip K^{TIP} governs the fracture process, so that the crack advances when $K^{\text{TIP}} = K^C$. Due to the transformation, K^{TIP} and K^{APP} will differ by an amount ΔK^{TIP}, defined through

$$K^{\text{TIP}} = K^{\text{APP}} + \Delta K^{\text{TIP}}, \tag{6}$$

where $\Delta K^{\text{TIP}} < 0$ if shielding occurs due to the transformation strains.

3. Constitutive equations

The constitutive equations used are based upon the assumption that we can identify a material sample which is small compared to all macroscopic dimensions, but which is large enough that statistical averaging over all transformable particles is meaningful. Such a material sample can then be treated as a continuum element for which all (macroscopic) quantities are averages over the sample. Phenomena on a smaller scale are discarded. This means, for instance, that local stress and strain fields around individual particles are not considered, but only the macroscopic average of these fields over all particles in the sample. Such macroscopic quantities will be indicated with uppercase letters.

When deriving the transformation plasticity model, Sun et al. [9] assume the continuum element to consist of a large number of transformable inclusions (referred to with index I) which are embedded coherently in an elastic matrix (referred to with index M). Microscopic quantities (on a lower scale then for which the continuum element is derived) will be referred to with lower case characters. The macroscopic quantities can be found by taking the volume average $\langle\ \rangle$ of the microscopic quantities over the element. For instance, the microscopic stress and strain tensors are indicated by $\boldsymbol{\sigma}$ and $\boldsymbol{\varepsilon}$, respectively, and with a given volume fraction of second phase (transformable metastable tetragonal inclusions) f^m, the relation between microscopic and macroscopic stresses $\boldsymbol{\Sigma}$ reads

$$\boldsymbol{\Sigma} = \langle\boldsymbol{\sigma}\rangle_V = \frac{1}{V}\int_V \boldsymbol{\sigma}\,\mathrm{d}V = f\langle\boldsymbol{\sigma}\rangle_{V_I} + (1-f)\langle\boldsymbol{\sigma}\rangle_{V_M}, \tag{7}$$

where the volume of the element, matrix and inclusions is given by V, V_M and V_I, respectively, and where f is the actual fraction of transformed material ($f < f^m$). The macroscopic strain $\boldsymbol{E}$ is assumed to be small, and considering isothermal deformations, can be decomposed into an elastic part $\boldsymbol{E}^e$ and a 'plastic' part $\boldsymbol{E}^p$ that is due to the $t \to m$ transformation in the inclusions, i.e.

$$\boldsymbol{E} = \boldsymbol{E}^e + \boldsymbol{E}^p = \boldsymbol{M}^0\boldsymbol{\Sigma} + f\langle\boldsymbol{\varepsilon}^p\rangle_{V_I}. \tag{8}$$

Here $\boldsymbol{M}^0 = (\boldsymbol{L}^0)^{-1}$, with $\boldsymbol{L}^0$ being the elastic moduli of both inclusions and matrix. The $t \to m$ phase transition may involve dilatation as well as shear strains within the inclusion, thus suggesting a split in the plastic strain into a dilatant part and a deviatoric part, designated with superscripts d and s, respectively,

$$\boldsymbol{E}^p = \boldsymbol{E}^{pd} + \boldsymbol{E}^{ps} = f\langle\boldsymbol{\varepsilon}^{pd}\rangle_{V_I} + f\langle\boldsymbol{\varepsilon}^{ps}\rangle_{V_I}. \tag{9}$$

The rates of plastic strain during progressive transformation ($\dot{f} > 0$) can be obtained by straightforward differentiation of (9); but they can also be obtained from the average of the transformation strain $\boldsymbol{\varepsilon}^p$ over the freshly transformed inclusions (per unit time) occupying volume $\mathrm{d}V_I$, i.e.

$$\begin{aligned}\dot{\boldsymbol{E}}^p = \dot{\boldsymbol{E}}^{pd} + \dot{\boldsymbol{E}}^{ps} &= \dot{f}\langle\boldsymbol{\varepsilon}^{pd}\rangle_{V_I} + \dot{f}\langle\boldsymbol{\varepsilon}^{ps}\rangle_{V_I} + \overline{\dot{f}\langle\boldsymbol{\varepsilon}^{pd}\rangle_{V_I}} + \overline{\dot{f}\langle\boldsymbol{\varepsilon}^{ps}\rangle_{V_I}} \\ &= \dot{f}\langle\boldsymbol{\varepsilon}^{pd}\rangle_{\mathrm{d}V_I} + \dot{f}\langle\boldsymbol{\varepsilon}^{ps}\rangle_{\mathrm{d}V_I}.\end{aligned} \tag{10}$$

The dilatant part $\boldsymbol{\varepsilon}^{pd}$ within each inclusion can be given in terms of the constant stress-free lattice volume dilatation ε^{pd}; hence,

$$\langle\boldsymbol{\varepsilon}^{pd}\rangle_{\mathrm{d}V_I} = \langle\boldsymbol{\varepsilon}^{pd}\rangle_{V_I} \equiv \boldsymbol{\varepsilon}^{pd} = \varepsilon^{pd}\boldsymbol{I}. \tag{11}$$

The average deviatoric part $\boldsymbol{E}^{ps}$ may be significantly smaller than the stress-free lattice shear strain due to the twinning effect. Based on the earlier work of Reyes–Morel and Chen [12], [13], this part is specified through its rate of change $\dot{f}\langle\boldsymbol{\varepsilon}^{ps}\rangle_{\mathrm{d}V_I}$, which is assumed to depend on the average deviatoric stress $\boldsymbol{s}^M$ in the matrix according to

$$\langle\boldsymbol{\varepsilon}^{ps}\rangle_{\mathrm{d}V_I} = A\frac{\boldsymbol{s}^M}{\sigma_e^M}, \qquad \sigma_e^M = \sqrt{\tfrac{3}{2}\,\mathrm{tr}(\boldsymbol{s}^M)^2}. \tag{12}$$

Here, A is a material function, which can be considered as a measure of the constraint of the elastic matrix on twinning, and σ_e^M is the von Mises stress in the matrix, which will be specified later. When $\sigma_e^M = 0, A$ should be put at zero because there is no stress bias. However, experimental data of [12], [13] show that under proportional loading the value of A is almost constant during the whole transformation process. Sun et al. [9] have emphasized that (12) is a macroscopic constitutive relationship that is assumed to apply to the ensemble of transformable particles mentioned in the beginning of the section. The deviatoric transformation strain over individual transformed particles will not depend on the local matrix stresses in such a simple manner. Firstly, twinning in a particle will occur in well-defined directions on specific crystallographic planes. Furthermore, the amount of twinning within particles is dependent on the particle size (see e.g. [19]). Although much research has been devoted to nucleation and twinning in a single particle, these are still phenomena which are not well understood and need further attention. However, since in this model many grains with different orientations are considered within $\mathrm{d}V_I$, Sun et al. [9] argue that (12) is an acceptable approximation in the average sense. Combining the expressions (10) to (12), the plastic strain-rate is found as

$$\dot{\boldsymbol{E}}^p = \dot{f}(\varepsilon^{pd}\boldsymbol{I} + \langle \boldsymbol{\varepsilon}^{ps} \rangle_{\mathrm{d}V_I}). \tag{13}$$

With the help of Eshelby's [20] solution for a spherical inclusion in an infinite extended elastic body and the method of Mori and Tanaka [21], the deviatoric and mean matrix stresses, $\boldsymbol{s}^M$ and σ^M respectively, are found to be

$$\boldsymbol{s}^M = \boldsymbol{S} - fB_1\langle \boldsymbol{\varepsilon}^{ps} \rangle_{V_I}, \qquad \sigma_m^M = \Sigma_m - fB_2\varepsilon^{pd}. \tag{14}$$

Here, $\boldsymbol{S} = \boldsymbol{\Sigma} - \Sigma_m\boldsymbol{I}$ and $\Sigma_m = \operatorname{tr}\boldsymbol{\Sigma}/3$ are the deviatoric and mean components of the macroscopic stress $\boldsymbol{\Sigma}$, and

$$B_1 = 2G\frac{5\nu - 7}{15(1-\nu)}, \qquad B_2 = 2B\frac{2\nu - 1}{1-\nu}, \tag{15}$$

with G the shear modulus, B the bulk modulus and ν the Poisson's ratio of the matrix as well as the inclusion, all being related in the standard way to Young's modulus E,

$$G = \frac{E}{2(1+\nu)}, \qquad B = \frac{E}{3(1-2\nu)}. \tag{16}$$

Finally, the transformation condition and the evolution relation in terms of $\dot{f}$ must be specified. Sun et al. [9] give the following condition for *forward* transformation $(+)$ to occur

$$\boldsymbol{F}_+(\boldsymbol{\Sigma}, f, T, \langle \boldsymbol{\varepsilon}^{ps} \rangle_{V_I}) = \tfrac{2}{3}A\sigma_e^M + 3\sigma_m^M\varepsilon^{pd} - C_0(T, f) = 0 \tag{17}$$

and

$$F_-(\boldsymbol{\Sigma}, f, T, \langle \boldsymbol{\varepsilon}^{ps} \rangle_{V_I}) = \tfrac{2}{3}A\sigma_e^M + 3\sigma_m^M\varepsilon^{pd} - \tilde{C}_0(T, f) = 0, \tag{18}$$

for *reverse* transformation $(-)$ to occur. The function $C_0(T, f)$ depends on the dissipation D_0 (due to i.e. interface friction), on the difference in surface energy A_0, on the free chemical

energy difference $\Delta G_{p\to m}(T)$ associated with the transformation (depending on the temperature T), and on the elastic energy associated with the interaction between transformed particles and matrix

$$C_0(T,f) = D_0 + A_0 + \Delta G_{p\to m}(T) - \tfrac{1}{3}B_1A^2 - \tfrac{3}{2}B_2(\varepsilon^{pd})^2 + \alpha B_0 f, \tag{19}$$

while

$$\tilde{C}_0(T,f) = C_0(T,f) - 2D_0. \tag{20}$$

The last term in (19) is introduced to incorporate the common experimental observation that the resistance to transformation tends to increase with increasing volume fraction of transformed material; here, this 'hardening' is governed by the parameter α. Note that this hardening term is due to processes on microstructural scale, such as

(i) particle size dependence: it takes a higher stress level to transform smaller particles;
(ii) crystallographic orientation: favorably oriented planes transform first, and
(iii) the mutual interference of transformed regions: transformation of a particle will cause a relaxation of the stresses in its surrounding.

As the constitutive model is derived for the macroscopic scale, considering many transformable particles in one constitutive element, the hardening effect did not follow from the derivation itself and Sun et al. [9] introduced the last term in (19) on mere phenomenological grounds. The parameter B_0 in (19) is a bulk modulus-like parameter defined by

$$B_0 = \frac{4G(1+\nu)(\varepsilon^{pd})^2}{1-\nu} + \frac{GA^2(28-20\nu)}{45(1-\nu)}. \tag{21}$$

The growth rate of the fraction transformed tetragonal phase, $\dot{f}$, follows from the consistency condition $\dot{F}_{+/-} = 0$, and is found as

$$\dot{f} = \frac{\langle \boldsymbol{\varepsilon}^{ps}\rangle_{\mathrm{d}V_I}\cdot\dot{\mathbf{S}} + 3\varepsilon^{pd}\dot{\Sigma}_m}{\frac{2}{3}B_1A^2 + 3B_2(\varepsilon^{pd})^2 + \alpha B_0}. \tag{22}$$

Expression (22) holds as long as the transformation progresses, i.e. when the current stress state satisfies the forward transformation condition (17) while the $t \to m$ transformation progresses, $\dot{f} > 0$, and there is still a transformable fraction left, $f < f^m$, or the current stress state satisfies the reverse transformation condition (18) while the $t \leftarrow m$ transformation progresses, $\dot{f} < 0$, and there is still a transformed fraction left, $f > 0$.

Finally, the constitutive equations will be rearranged into a form which is necessary for the subsequent numerical analysis. After differentiating (8), and combining with (10)–(12), one can derive the following rate constitutive equations

$$\dot{\boldsymbol{\Sigma}} = \boldsymbol{L}\dot{\boldsymbol{E}}, \tag{23}$$

with the tensor of instantaneous moduli $\boldsymbol{L}$ being defined by

$$\boldsymbol{L} = \begin{cases} \boldsymbol{L}^0 - \dfrac{1}{g}\dfrac{\boldsymbol{L}^0\boldsymbol{T}\otimes\boldsymbol{T}\boldsymbol{L}^0}{1+\frac{1}{g}(\boldsymbol{T}\cdot\boldsymbol{L}^0\boldsymbol{T})} & \text{when} \quad F_+ = 0 \ \text{ and } \ \dot{f} > 0, \ \text{ or} \\ \qquad\qquad\qquad\qquad\qquad\quad F_- = 0 \ \text{ and } \ \dot{f} < 0; \\ \boldsymbol{L}^0 \quad \text{when} \quad F_+ \neq 0 \ \text{ or } \ \dot{f} < 0, \ \text{ or} \\ \qquad\qquad\quad F_- \neq 0 \ \text{ or } \ \dot{f} > 0 \end{cases}, \tag{24}$$

where

$$\boldsymbol{T} \equiv \varepsilon^{pd}\boldsymbol{I} + A\frac{\boldsymbol{s}^M}{\sigma_e^M}, \qquad g \equiv \tfrac{2}{3}B_1A^2 + 3B_2(\varepsilon^{pd})^2 + \alpha B_0(\varepsilon^{pd})^2. \tag{25}$$

Details may be found in [22]. On the transformation branch, the stiffness tensor $\boldsymbol{L}$ is comprised of the linear elastic stiffness tensor $\boldsymbol{L}^0$ and a nonlinear part due to the transformation which is similar to the plastic moduli in elastoplasticity. Note that the moduli $\boldsymbol{L}$ possess the following symmetry when expressed in their Cartesian components L_{ijkl}

$$L_{ijkl} = L_{klij}, \tag{26}$$

in addition to the obvious symmetries in ij and kl (see [14]).

4. Numerical method

As mentioned in Section 2.1, this part will address crack growth in cases where the transformable phase is distributed symmetrically with respect to the plane $x_2 = X_2 = 0$, so that on the basis of symmetry, the propagating crack will remain in that plane. Under these symmetry conditions, the analysis can be confined to only one-half of the region in the small-scale transformation problem shown in Figure 3.

A displacement-based finite element method is used to solve the small scale transformation, boundary value problem described in Section 2.2. The implementation of the constitutive equations for the Sun et al. [9] transformation model makes use of the similarity between their formulation (23)–(24) and the usual time-independent elastoplasticity equations with an associative flow rule. The resulting finite element equations for the displacement rates are solved in a linear incremental manner, as described in some detail in [14].

In the finite element analysis, quadrilateral elements are used, each of which is built up of four constant strain elements. The mesh that has been used for the symmetric problem under consideration here is shown in Figure 4, and contains 2770 quadrilateral elements and 2880 nodes. Displacement boundary conditions are prescribed on the circular outer boundary in accordance with the applied stress intensity factor K^{APP}. The mesh is designed such that the mesh is highly refined near the tip, as shown in Figure 4c. At the start, the crack tip is placed at three elements to the right of the left-hand side of the rectangular region of the mesh. Crack growth is simulated by using a nodal release technique similar to the method used by Hom and McMeeking [25]. The nodal force at the current crack-tip node position is stepped down to zero in five increments, and the displacement boundaries at the outer radius are adjusted to the new position relative to the moved tip. Crack growth was permitted over a span of 80 nodes to the right-hand side of the mesh.

The stress intensity at the crack tip K^{TIP} can be calculated with (6). The value of ΔK^{TIP}, compared to the critical value for propagation $K^{\mathrm{TIP}} = K^C$, determines the toughness enhancement due to transformation. This toughness enhancement can be conveniently calculated using a method developed by Hutchinson [23], which leads to

$$\Delta K^{\mathrm{TIP}} = \int_A \int \frac{1}{\sqrt{8\pi}} \frac{E}{(1-\nu^2)} r^{-3/2} M(E^{\mathrm{p}}_{\gamma\delta}, \beta)\, \mathrm{d}A, \tag{27}$$

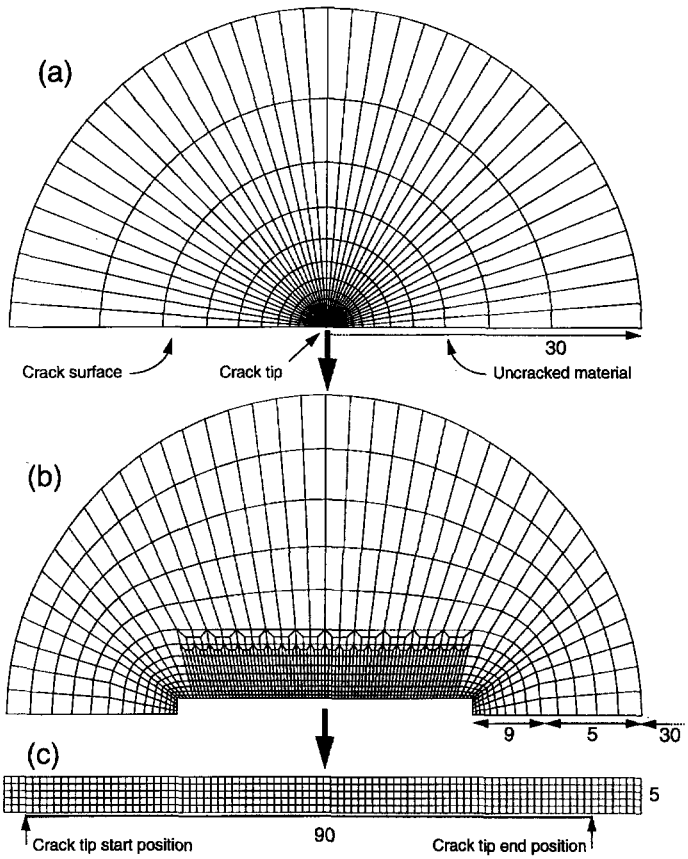

Figure 4. The finite element mesh used to analyze the small-scale crack-growth problem. The mesh comprises 2770 quadrilateral elements and 2880 nodes. Crack growth by nodal release is permitted to occur over a span of 80 nodes.

where r and β are polar coordinates from the crack tip (see Figure 3), A is the upper half of the transformation zone and $M(E^p_{\gamma\delta}, \beta)$ is given by Lambropoulos [24] as

$$M(E^p_{\gamma\delta}, \beta) = (E^p_{11} + E^p_{22})\cos\frac{3\beta}{2} + 3E^p_{12}\cos\frac{5\beta}{2}\sin\beta + \tfrac{3}{2}(E^p_{22} - E^p_{11})\sin\beta\sin\frac{5\beta}{2}. \quad (28)$$

Here, $E^p_{\gamma\delta}$ are the in-plane transformation strains that would occur under plane strain conditions in the absence of in-plane stresses, i.e. $\Sigma_{\gamma\delta} = 0$ with $E_{i3} = 0$. With the general 3-D transformation strain $\boldsymbol{E}^p$ in each spot being given by (9), it follows from constitutive relation (8) in plane strain that the resulting nonzero strains are given by

$$E^p_{11} = (1+\nu)f\varepsilon^{pd} + f[\langle\varepsilon^{ps}_{11}\rangle_{V_I} - \nu(\langle\varepsilon^{ps}_{11}\rangle_{V_I} + \langle\varepsilon^{ps}_{22}\rangle_{V_I})],$$

$$E^p_{22} = (1+\nu)f\varepsilon^{pd} + f[\langle\varepsilon^{ps}_{22}\rangle_{V_I} - \nu(\langle\varepsilon^{ps}_{11}\rangle_{V_I} + \langle\varepsilon^{ps}_{22}\rangle_{V_I})].$$

$$E^p_{12} = f\langle\varepsilon^{ps}_{12}\rangle_{V_I}. \quad (29)$$

The value of ΔK^{TIP} is computed numerically on the basis of the integral formulation (27) and (28), with a 13 point Gaussian-integration within each element. However, near the crack

tip the integration is carried out analytically to take care of the singularity in (27) at the tip. Further details may be found in [14].

5. Results

The analysis of the effect of non-homogeneously distributed transformable phase on the toughness development during crack growth is similar to the previously presented analyses in [14, 15, 16]. To facilitate the comparison with previous results, the same set of non-dimensional parameters is used to characterize the crack-growth problem. However, two parameters are added to characterize the heterogeneity, namely the amplitude C_A and the non-dimensional characteristic period of the heterogeneity

$$\lambda_c = L_c/L. \tag{30}$$

Here L is a characteristic length which is used to scale all lengths, and is defined by

$$L \equiv \frac{2}{9\pi}\left[\frac{K^C\{h_0(1-2\nu)+(1+\nu)\}}{\Sigma^C}\right]^2, \tag{31}$$

with

$$h_0 \equiv \frac{A}{3\varepsilon^{pd}}, \qquad \Sigma^C \equiv \frac{C_0(T)}{3\varepsilon^{pd}}. \tag{32}$$

Physically, L represents the distance on the x_1-axis from the tip to the boundary of the transformation zone just before crack growth, when for the determination of the transformation zone, the undisturbed elastic field is taken ($K^{\text{APP}} = K^C$), as shown in [22]. The strength of the transformation ω is defined in [14] by

$$\omega \equiv \frac{3Ef^m\varepsilon^{pd}(1+\nu)}{\Sigma^C(1-\nu)} \tag{33}$$

and the definition for M, the parameter which governs the reversible transformation behavior, is defined in [26] as

$$M \equiv \frac{\tilde{C}_0(T,f)}{C_0(T,f)}. \tag{34}$$

Thus, the deformation response can be expressed in the following set of non-dimensional parameters: the Poisson ratio ν, the linear hardening coefficient α, the strength of the transformation ω, the amount of transformation shear strain h_0, the reverse transformation parameter M, and the amplitude and period of the periodical distribution function, C_A and λ_c

$$\nu, \alpha, \omega, h_0, M, C_A, \lambda_c. \tag{35}$$

In [14] it was shown how to determine the values of the parameters ν, α, ω, h_0 from stress-strain curves obtained by triaxial compression tests. The hydrostatic pressure of about 120 MPa makes it possible to reach relatively large deformations and loading levels before the specimen fails. From such stress-strain curves reported in [12, 13], it was found that for PSZ at room

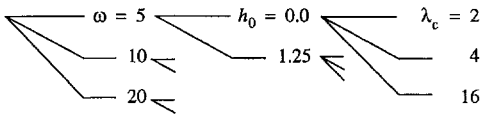

Figure 5. The parameter combinations that have been taken for the computations.

temperature: $\nu = 0.3, \alpha = 1.16, \omega = 24, h_0 = 1.4$ while for TZP: $\nu = 0.3, \alpha = 1.2, \omega = 11, h_0 = 1.3$. We have not been able to locate such triaxial stress-strain curves for ZTA material in the open literature. Therefore, we perform a parameter study here, and shall assume that the values for ZTA are in the range of the values for PSZ and TZP.

For the purpose of this study, it is sufficient to consider variations only of the parameters ω, h_0 and λ_c, since we are especially interested in how the crack-growth behavior is influenced by a non-uniform distribution of transformable phase f^m. The remaining parameters have been set to constant values: $\nu = 0.3, \alpha = 1.15, M = -\infty$ and $C_A = 1$, describing a ZTA material with realistic Poisson ratio and hardening, and with no reversible transformation. The effect of reverse transformation in homogeneous materials has been studied in [26]. There it was concluded that reverse transformation always reduces the toughening. In this first part of the paper, we do not simulate crack growth in materials with reverse transformation, but in Part II [1] we will investigate the influence of reversibility of the transformation on the crack-deflection behavior. Qualitatively, the influence of C_A is clear; a reduction of C_A simply means that the material becomes less heterogeneous and when the value of C_A approaches zero, the results approach the results for homogeneous materials presented in e.g. [14]. A maximal influence of the heterogeneous distribution is obtained for $C_A = 1$.

In conformity with the range of variation in previous studies [14, 15, 25] the value of the strength of the transformation ω has been set to 5, 10 or 20. The amount of transformation shear strain has been set to the realistic value $h_0 = 1.25$, or to $h_0 = 0$ in order to simulate purely dilatant transformation behavior (cf. [10, 11, 14]).

Finally, for ZTA, the key parameter in this context, λ_c, has been set to 2, 4 or 16. These values were chosen on the basis of the plot at the right-hand side of Figure 1, which gives a cross-section of the transformation zone perpendicular to the crack in ZTA according to [17]. From this, we estimate the period of the heterogeneities to be of the order of the height of the transformation zone. Hence, varying λ_c in the range of 2 to 16 seems reasonable. For Duplex Ceramics, we have chosen for particle sizes in the order of the height of the transformation zone, by taking $\lambda_c = 0.56, 1.12$ or 4.48.

For an overview of the sets of parameters which we have taken for the parameter study, we refer to Figure 5. The results of the parameter study are presented in Figures 7 to 10, and in Figures 11 and 12 for duplex materials. Each figure corresponds to a particular combination of ω and h_0, and demonstrates the influence of the distribution parameter λ_c. The results of the computations are presented in terms of transformation zones and predicted crack-growth resistance curves.

5.1. TRANSFORMATION ZONES

ZTA

A contour line representation of the fraction f of transformed material is used to visualize the transformation zones surrounding the crack. It is emphasized that no attempt has been made

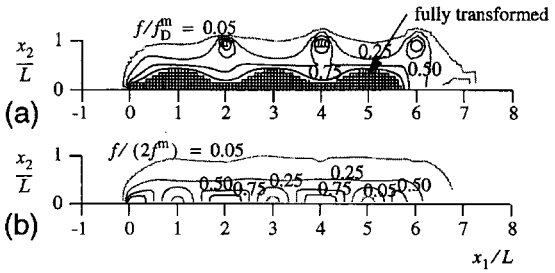

Figure 6. Different contour line representations of the transformed material surrounding the crack tip when $\Delta a = 533L$ for $\omega = 5, h_0 = 0.0$ and $\lambda_c = 2$, obtained through normalization by (a) the local, available transformable fraction $f_D^m = f_D^m(X_1, X_2)$, and (*b*) by the maximum transformable fraction $2f^m$. The hatched region in (a) indicates the elements in which all material has transformed.

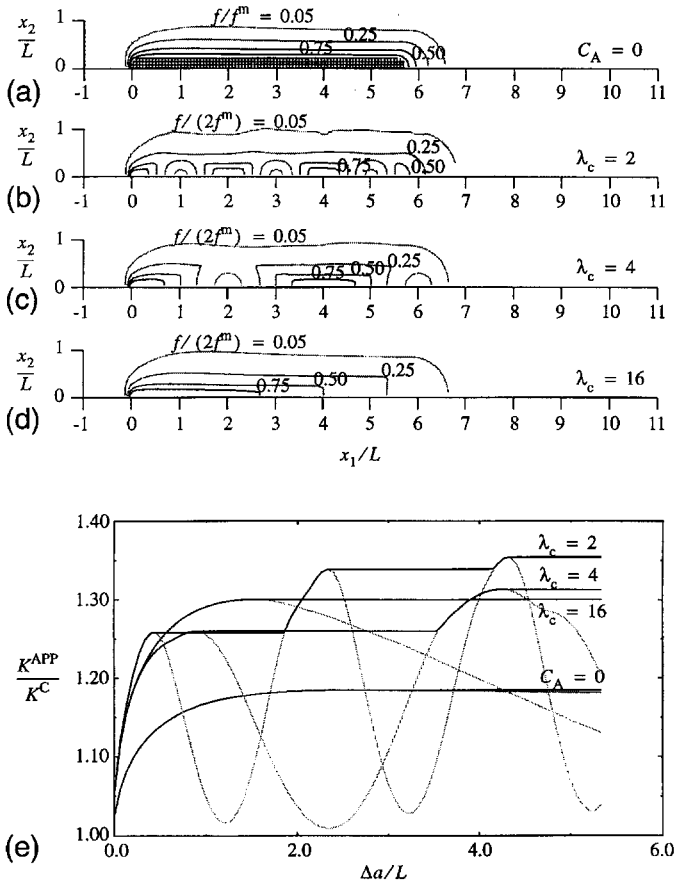

Figure 7. Transformation zones (a to d) when $\Delta a = 5.33L$, and the crack-growth resistance curve, and (e) for material parameters $\omega = 5, \alpha = 1.15, h_0 = 0.0$ and for a distribution according to (2) with $\lambda_c = 2$ to 16.

to smooth the contours. For non-homogeneous distributions of transformable fractions, there are various ways of normalizing the results. When we use contour lines of constant value of the ratio of a current transformed fraction to a locally available transformable fraction, $f/f_D^m(X_1, X_2)$, we obtain plots like Figure 6a. This may be a suitable way of representing the numerical results, but it suffers from two drawbacks. First, it is not convenient to compare

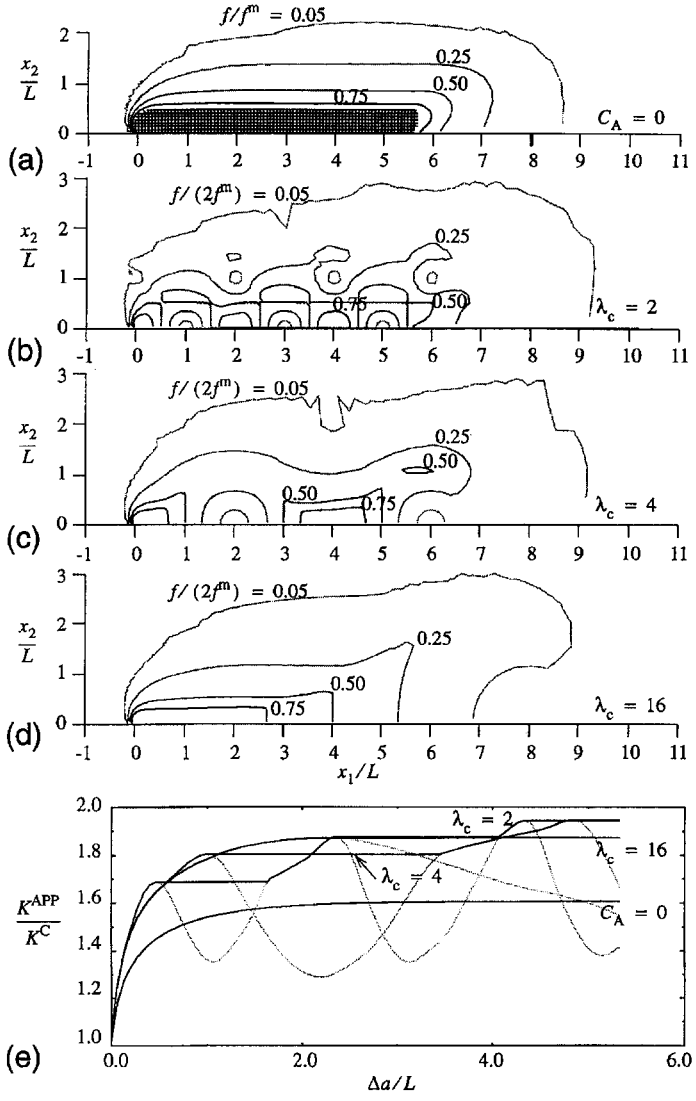

Figure 8. Transformation zones (a to d) when $\Delta a = 5.33L$, and the crack-growth resistance curve, and (e) for material parameters $\omega = 5, \alpha = 1.15, h_0 = 1.25$ and for a distribution according to (2) with $\lambda_c = 2$ to 16.

the zones to experimental results, because in reality the available transformable phase is not distributed according to some known function. Second, it tends to emphasize the regions of low available fractions. Adjacent to the crack plane in Figure 6a we observe a zone of oscillating width where the material is fully transformed; the greatest width of that zone corresponds to a region where $f_D^m(X_1, X_2)$ is low. Also regions of low-transformable fractions slightly away from the fracture plane appear highlighted because of the normalization.

Therefore, we have chosen to scale the current transformed fraction f with 'the maximum transformable fraction' $(1 + C_A)f^m$. As $C_A = 1$ in all computations reported here, the new ratio becomes $f/(2f^m)$, with which the same results as in Figure 6a now appear as in Figure 6b. Note that now it is no longer clear that the material next to the crack is fully transformed.

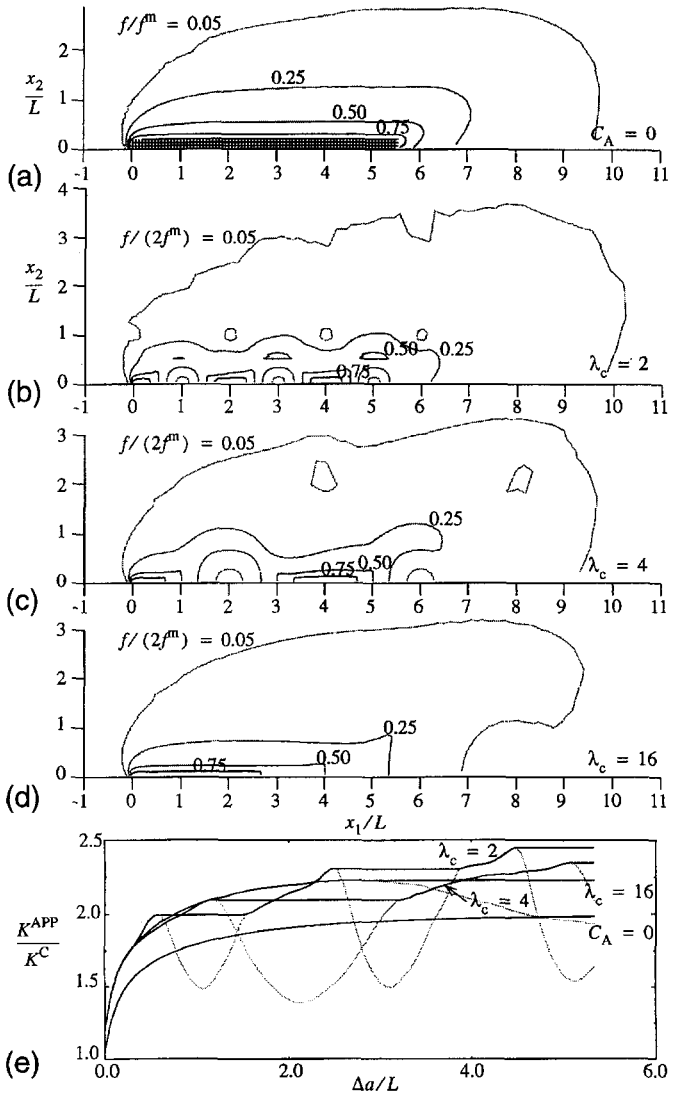

Figure 9. Transformation zones (a to d) when $\Delta a = 5.33L$, and the crack-growth resistance curve, and (e) for material parameters $\omega = 10, \alpha = 1.15, h_0 = 1.25$ and for a distribution according to (2) with $\lambda_c = 2$ to 16.

For the purpose of comparison, the plots (a) in Figures 7 to 10 also show the transformation zones as if the transformable phase were homogeneously distributed as in [14, 15]. Notice that when comparing the transformation zone plots for homogeneous distributions with those for the heterogeneous distributions (plots (b), (c) and (d) of the same figure range), the maximum transformable phase available locally is twice as large as that in the latter case (recall that f^m is the average available transformable fraction). For all cases, transformation zones are shown after the crack has grown over a distance $\Delta a = 5.33L$, which for homogeneous materials corresponds well with a steady state.

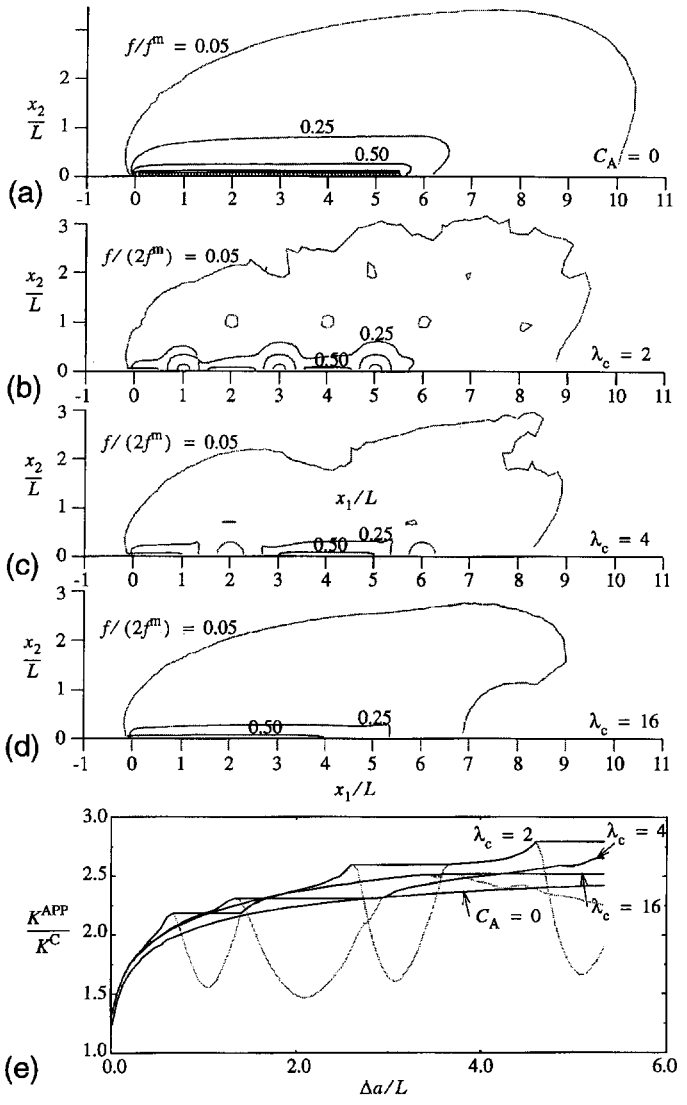

Figure 10. Transformation zones (a to d) when $\Delta a = 5.33L$, and the crack-growth resistance curve, and (e) for material parameters $\omega = 20, \alpha = 1.15, h_0 = 1.25$ and for a distribution according to (2) with $\lambda_c = 2$ to 16.

Evidently, the structure of the transformation zones are inherited from the distribution of the transformable phase. For $f_D^m(X_1, X_2)$ as in (2), we see that the minima of f_D^m have a value of $(1 - C_A)f^m$ and are located at

$$\frac{X_1}{L} = \frac{x_1}{L} = \frac{(1+j)+2i}{2}\lambda_c, \qquad \frac{X_2}{L} = \frac{x_2}{L} = \frac{j}{2}\lambda_c, \tag{36}$$

for i and j being integers. The pattern of minima is clearly traceable in all contour plots in Figures 7 to 10. The areas with minimum content of transformable phase are surrounded by transformed material and therefore the contour $f/(2f^m) = 0.05$ encircles such minima. A clear example of such a pattern can be seen in plot (b) of Figure 8. The distance between the minima increases when λ_c increases (cf. (36)), which is demonstrated in plot (c) and (d) of Figure 8.

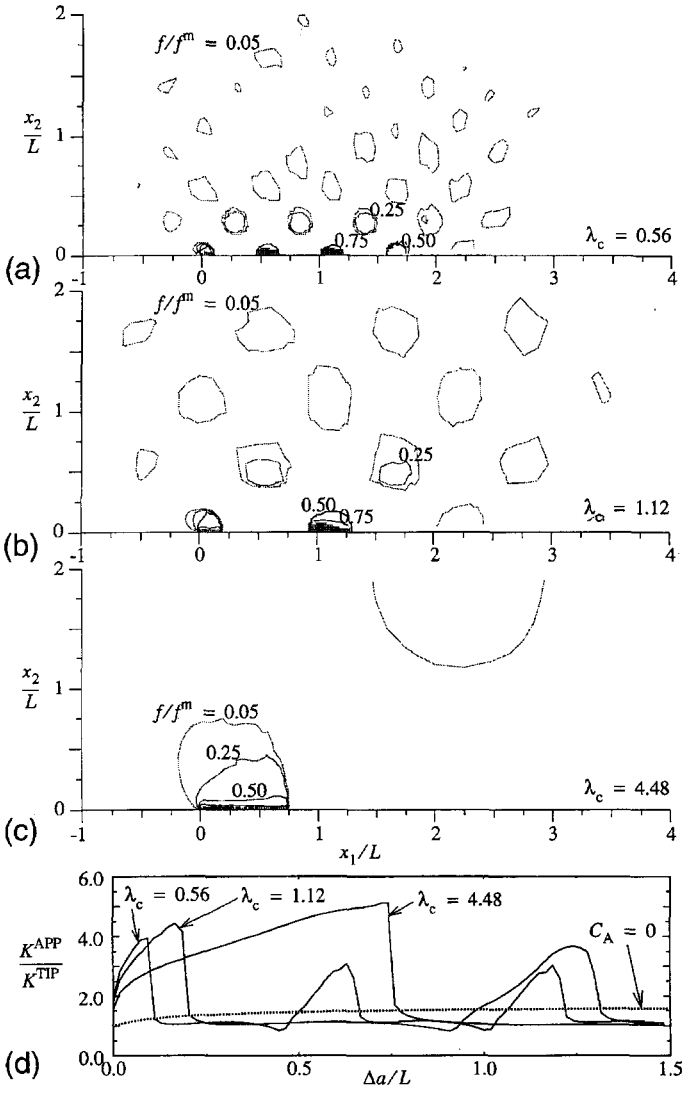

Figure 11. Transformation zones (a to c) when $\Delta a = 1.48L$, and the crack-growth resistance curve, and (d) for a duplex material with parameters $\omega = 5, \alpha = 1.15, h = 1.25$ and a distribution (3) with $\lambda_c = 0.56$ to 4.48.

Further examination of Figures 7 to 10 reveals that the distribution parameter λ_c has only a minor effect on the 'overall height' of the transformation zone, as laid out by the $f/(2f^m) = 0.05$ contour. Thus, the transformation zone height for the present material parameters is essentially independent of the distribution of the transformable phase. However, the shape of the transformation zone is changed considerably for various values of λ_c. The change in shape is most pronounced near the crack surface. There, the limit of available transformed fraction, $f_D^m(X_1, X_2)$ is often reached, while further away from the crack surface the transformed fraction is so low that the maximum limit is not reached. In that region, only the absolute minima, as indicated through (36) may affect the shape. This is clearly shown in the plots (b) of Figures 8, 9 and 10, and to somewhat lesser extent in plots (c) and (d) of the same figures. Comparing Figure 8 with Figure 7, where the transformation is assumed to be

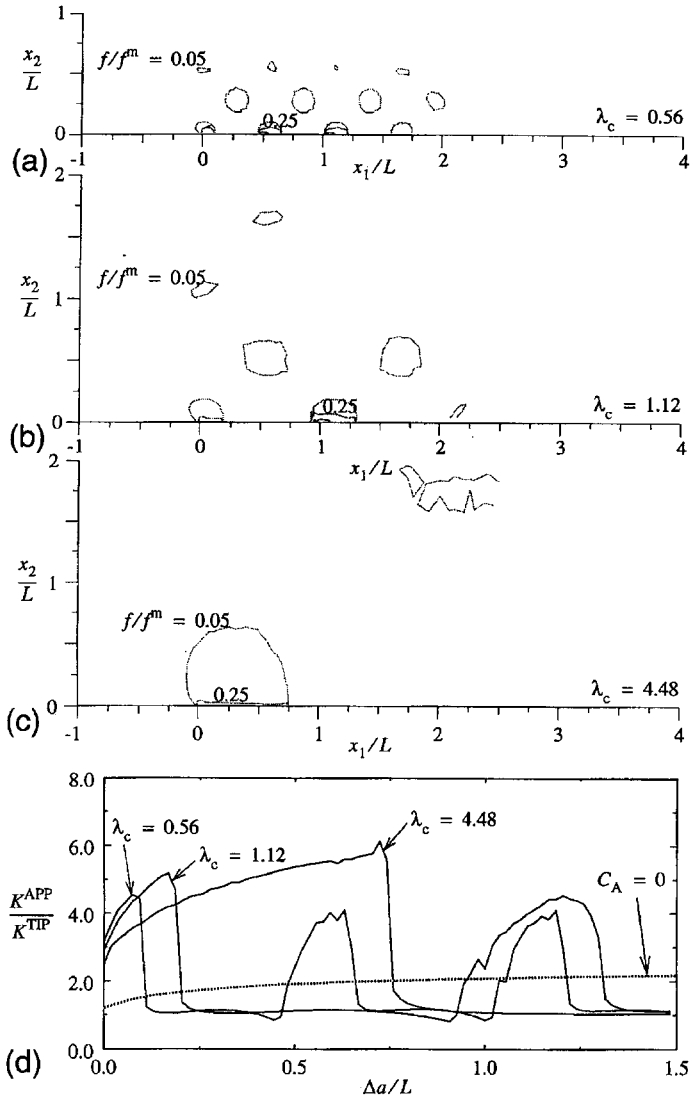

Figure 12. Transformation zones (a to c) when $\Delta a = 1.48L$, and the crack-growth resistance curve, and (d) for a duplex material with parameters $\omega = 20$, $\alpha = 1.15$, $h = 1.25$ and a distribution (3) with $\lambda_c = 0.56$ to 4.48.

purely dilatant, we see that the transformation shear effect tends to enhance the distortion of the transformation zones through the heterogeneous distribution of transformable phase.

Duplex Ceramics

Again a contour plot representation is used to visualize the transformation zones in Figures 11 and 12. The contours show lines of constant ratio $f/f^{\max}$ where for duplex materials $f^{\max} = 1$ inside the inclusions. As the crack propagates, more inclusions transform and a zone of transformed inclusions can be seen. It should be noted that none of the inclusions has transformed completely. The smallest inclusions ($\lambda_c = 0.56$ in plot (a)) of both Figures 11 and 12 at the crack surface are almost fully transformed. Further away from the crack

surface the inclusions are 25 percent transformed, followed by a zone in which the inclusions are transformed for only 5 percent.

Evidently, for duplex materials, there is not a smooth transformation zone surrounding the propagating crack. Rather, the contour plots directly reflect the discrete pattern at which the inclusions are laid out. For the chosen crack path A, the centers of the inclusions are located at

$$\frac{X_1}{L} = \frac{x_1}{L} = \frac{j+2i}{2}\lambda_c, \qquad \frac{X_2}{L} = \frac{x_2}{L} = \frac{j}{2}\lambda_c, \tag{37}$$

for i and j being integers.

5.2. Crack growth resistance

ZTA

The computed crack-growth resistance for these types of materials is presented in the plots (e) of Figures 7 to 10, in terms of the applied stress intensity factor $K^{\mathrm{APP}}(\Delta a)$ scaled by the critical stress intensity factor K^C as a function of the crack advance Δa relative to the material length parameter L. Crack growth occurs if the stress intensity at the crack tip reaches the critical stress intensity, $K^{\mathrm{TIP}} = K^C$. When the applied stress intensity, K^{APP}, has to be raised above the critical stress intensity in order to enforce crack growth, it must be concluded that the transformation strains shield the crack tip and the apparent toughness has been increased.

Similar to previous results for homogeneous materials [11, 14, 15] it is found that, prior to crack growth, the transformation strains hardly influence the stress intensity at the tip. However, upon crack growth, we find that K^{APP} needs to be increased considerably, before the critical stress intensity at the tip is reached and crack growth proceeds. Moreover, we see that the development of the toughness during crack growth is strongly affected by the introduction of heterogeneity. In all the results presented in Figures 7 to 10, the initial position of the crack tip is situated in the centre of a rich area, where the amount of transformable strain is twice the average value. Therefore, the toughening develops more rapidly than for a homogeneous material ($C_A = 0$).

Upon crack growth the tip moves into an area where the distribution function D reaches a minimum, so that the available transformable phase is small. In accordance with that, we find that the toughness reaches a local maximum, because upon further crack growth, the shielding effect of the transformation strains reduces: stress intensity is found which is larger than the critical stress intensity. Without further loading, more nodes are released in the numerical computation as long as $K^{\mathrm{TIP}} \geqslant K^C$, until the shielding effect returns to its value of the local maximum. Subsequently, the applied stress intensity needs to be raised further for crack propagation until a region with a relatively low amount of transformable phase is hit again. Hence, contrary to K^{APP}/K^C, $K^{\mathrm{APP}}/K^{\mathrm{TIP}}$ would appear as an oscillating function of Δa, as shown in grey in the figures. As expected, the period of the oscillations is proportional to the value of λ_c.

It is evident that an oscillating crack-growth resistance is a computational artifact. In reality, unstable crack growth occurs once $K^{\mathrm{APP}}/K^{\mathrm{TIP}}$ reaches a maximum, and the crack grows dynamically until it arrests at a transformation rich area. Our simulation assumes quasi-static behaviour, and the horizontal parts in the resistance curves must be seen as unstable, without practical value.

The results in Figures 7 to 10 show that the peak values of the toughness increase with each pass of the crack tip through a relatively rich region; but, the increase seems to saturate with continued grack growth. When comparing the results with those for a homogeneous material with the same average transformable fraction, we observe that the maximum crack-resistance is in all cases larger. However, the improvement of this maximum value over the toughness for the homogeneous material depends on ω: the improvement decreases with increasing strength ω of the transformation. For example, for $\omega = 5$ in Figure 8e, we see that the increase for $\lambda_c = 2$ is more than 60 percent, while for $\omega = 20$ in Figure 10e, the increase is hardly 25 percent. Furthermore, the results suggest that for decreasing λ_c, the maximal toughness value increases. It must be noted, however, that the simulations involved only a limited amount of crack growth, so that for the larger values of λ_c there is an increased likelihood that the maximum (steady state) value for the toughness has not been reached. However, further crack growth would require a larger mesh and the computations would become too time-consuming.

When the starting position of the crack tip is at the centre of an area with a small fraction of transformable phase ($x_1/L = X_1/L - \lambda_c/2, x_2 = X_2$), the increase in toughness develops more slowly compared to the results for homogeneous materials. But after the somewhat slower start, the toughness development takes place in a similar manner to those where the starting position is inside a rich area. Therefore, these results are not presented separately here.

Duplex Ceramics

Similar to the results for ZTA materials, Figures 11 and 12 (plots (d)) demonstrate a toughening behavior for duplex material that varies strongly with the amount of crack growth. The peak toughness values are much higher then the peak toughness for material where the toughness is distributed homogeneously ($C_A = 0$). The evolution of the toughness can be explained by looking at the position of the inclusions. Initially, in these computations, the crack tip is located in the center of an inclusion. As the load increases, the material in the inclusion starts to transform. As the crack propagates, more transformed material enters into the wake of the crack. Usually, transformation strains behind the crack tip (at least in a fan $\beta > \pi/3$ in Figure 3) have a positive effect on the toughening (e.g. [11, 26]). Subsequently, when the crack has cleaved the inclusion, the toughness drops dramatically, showing that transformation strains in the immediate vicinity of the crack tip influence the stress intensity at the crack tip most (cf. [26]). After this drop, the toughness is close to the fracture toughness of the untransformed matrix material, while the toughness may become even lower than that as the tip approaches the next inclusion. The reason for this is that the transformation strains in a fan $\beta < \pi/3$ ahead of the tip usually have an embrittling effect. As soon as the tip grows into the inclusion, the toughness increases again. Evidently, in practice the crack would grow dynamically after it passed through an inclusion, and it would only stop if a subsequent peak in the toughness development curve is higher. To emphasize this unstable crack growth, the crack-growth resistance has been plotted in Figures 11 and 12 by way of the ratio $K^{\mathrm{APP}}/K^{\mathrm{TIP}}$. This is similar to the previous oscillatory $K^{\mathrm{APP}}/K^{\mathrm{TIP}}$ response indicated in Figures 7 to 10.

It is clear from the foregoing explanation that the distance between toughness peaks is directly linked to the value of the spacing between inclusions, as governed by λ_c. Further, we observe from Figures 11 and 12 that the height of the first toughness peak increases with increasing λ_c, since the size of the transforming inclusions scale with λ_c. This initial, more or less artificial, size scale effect is seen to essentially disappear after the crack has propagated to neighbouring inclusions. Finally, we note that an increase in the strength of the transformation,

ω, leads to higher peak toughnesses, but the development of the toughness during crack growth remains equal.

6. Discussion

From the numerical crack growth simulations reported here, where the crack has been constrained to remain in a predetermined plane, we can conclude that a heterogeneous distribution of transformable phase may give rise to an increase in toughness, compared to materials with a perfectly homogeneous distribution of ZrO_2. Although the actual cause cannot easily be made precise, we think that the effect is due to the fact that the transformed material is more 'clustered' right behind in the wake of the crack. Although the effect diminishes for larger values of the strength of the transformation, ω, it certainly seems to be an improvement for the toughness of the material.

The trend is emphasized in our results for Duplex materials, where, as a limiting case of a heterogeneous distribution, all transformable material is fully concentrated in clusters. There, we find that the crack is strongly held up by the clusters of transformable phase. When that occurs, we find a dramatic increase in peak toughness compared with the corresponding homogeneous material with the same volume fraction of transformable material. Confronting the Duplex results in Figures 11 and 12 with the Figures 8 and 9, respectively, for the corresponding cases with a smoother distribution, it is seen that the concentration in clusters actually improves the toughness by a factor of 2 to 2.5. These findings, in retrospect, may motivate the practical development of Duplex materials where relatively large (10–50 μm) spherical t-ZrO_2 zones are dispersed in a ceramic matrix, as discussed in [5, 27, 28]. For these materials, experiments show that the toughness is increased, but the strength of the material is decreased, compared to conventional ZTA materials.

Lutz and Claussen [5] distinguish between two types of toughening behavior in duplex materials: short-range and long-range behaviour, respectively. Short-range toughened materials exhibit a less broad load maximum than the long-range materials where toughness increase is found up to a 2 mm crack extension. It seems that the results presented here are best compared to short-range toughened ceramics with a high density. The crack growth behavior in these materials is characterized by a fairly straight-growing crack with a narrow zone of transformed inclusions close to the crack surface, and microcracking does not occur [5].

Obviously, the above findings have to be seen in relation with the model assumptions. An obvious factor is the assumed symmetry of the problem and therefore, the required symmetry of the heterogeneous distribution. This problem is studied in Part II [1]. Another factor is the particular periodic distribution of the transformable phase that has been assumed in (2). Given that distribution, also the pre-determined crack path will have an affect on toughening. To get some insight in this effect, a few analyses are carried out in [22] for two diagonal paths in the distribution shown in Figure 2: one starting at a peak in the distribution ($X_1 = X_2 = 0$), the other starting from a dip ($X_1 = L_c/2, X_2 = 0$). For both paths, lower values of the toughness are found, but the reduction is limited to only about 5 percent.

Apart from the symmetry with respect to the crack plane, the results should also be expected to depend on the fact that the distributions of transformable phase have been taken to be doubly-periodic. With reference to Figure 1, this is clearly an idealization. However, at the moment, performing similar studies for randomly distributed transformable phase would require too much computation time: a large number of computations is required before any

statistically meaningful conclusions can be drawn and, since each crack-growth simulation required about 100 CPU hours on a SUN Sparc-1 workstation, this is currently not feasible.

It should also be noted that crack growth in our analyses has been permitted only over a fixed distance. It may well be that the maximum reported toughness is not the maximal achievable toughness: a larger value for K^{APP}/K^{C} may be found upon further crack growth. It appeared, however, that the computer time and memory, required for such computations are still too large.

In the derivation of the continuum model (see Section 3), it is assumed that a material element contains many grains. However, especially in ZTA materials, the transformation zone only spans a few grains, so that the validity of the continuum approach may be questionable in some cases. This also limits our approach to the investigation of the influence of areas with varying transformable phase, and excludes the study of the influence of very large particles or flaws on the deformation behavior. Once more we want to stress that we assumed that microcracks do not exist before crack growth, and do not develop during the crack-growth simulation. Instead, the transformable particles remain coherently embedded in the matrix.

Acknowledgements

The work of Geert Stam was made possible by the Netherlands Organization for Scientific Research (NWO).

References

1. G.Th.M. Stam and E. van der Giessen, Crack growth in non-homogeneous transformable ceramics. Part II: Crack deflection, *International Journal of Fracture* 79 (1996) 273–293.
2. A.G. Evans and A.H. Heuer, *Journal of the American Ceramics Society* 63 (1980) 241–248.
3. D.J. Green, R.H.J. Hannink and M.V. Swain, *Transformation Toughening of Ceramics*, CRC Press, Boca Raton, Florida, USA (1991).
4. M. Rühle, N. Claussen and A.H. Heuer, *Journal of the American Ceramics Society* 69 (1986) 195–197.
5. E.H. Lutz and N. Claussen, *Journal of the American Ceramics Society* 74 (1991) 11–18.
6. A.G. Evans, N. Burlingame, M. Drory and W.M. Kriven, *Acta Metallurgica* 29 (1981) 447–456.
7. B. Karihaloo, in *Structural Ceramics Processing, Microstructure and Properties.*, J.J. Bentzen et al. (eds.), Riso, Denmark (1990) 359–364.
8. P. Den Exter, *Synthesis, Microstructure and Mechanical Properties of Zirconia–Alumina Composites.* Ph.D. thesis, Enschede, The Netherlands (1991).
9. Q.P. Sun, K.C. Hwang and S.U. Yu, *Journal of Mechanics and Physics of Solids* 39 (1991) 507–524.
10. R.M. McMeeking and A.G. Evans, *Journal of the American Ceramics Society* 65 (1982) 242–246.
11. B. Budiansky, J.W. Hutchinson and J.C. Lambropoulos, *International Journal of Solids and Structures* 19 (1983) 337–355.
12. P.E. Reyes-Morel and I.W. Chen, *Journal of the American Ceramics Society* 71 (1988) 343–353.
13. I.W. Chen and P.E. Reyes-Morel, *Journal of the American Ceramics Society* 69 (1986) 181–189.
14. G.Th.M. Stam, E. Van der Giessen and P. Meijers, *International Journal of Solids and Structures* 31 (1994) 1923–1948.
15. G.Th.M. Stam and E. Van der Giessen, in *Fracture Mechanics*; 25th volume, *ASTM STP 1220*, F. Erdogan and R.J. Hartranft (eds.), Philadelphia, USA (1995) 3–18.
16. G.Th.M. Stam, E. Van der Giessen and P. Meijers, *Materials & Design* 14 (1993) 83–86.
17. M. Rühle, A. Strecker, D. Waidelich and B. Kraus, *Journal of the American Ceramics Society* 12 (1984), 256–274.
18. M. Rühle and A.G. Evans, *Progress in Material Science* 33 (1989) 85–167.
19. A.G. Evans and R.M. Cannon, *Acta Metallurgica* 34 (1986) 2435–2441.
20. J.D. Eshelby, *Progress in Solid Mechanics II*, I.N. Sneddon and R. Hill (eds.) (1961) 89–140.
21. T. Mori and K. Tanaka, *Acta Metallurgica* 21 (1973) 571–574.
22. G.Th.M. Stam, *A Micromechanical Approach to Transformation Toughening in Ceramics*, Ph.D. thesis, Delft University of Technology (1994).
23. J.W. Hutchinson, *Harvard University Report TR74–1042* (1974).

24. J.C. Lambropoulos, *International Journal of Solids and Structures* 22 (1986) 1083–1106.
25. C.L. Hom and R.M. McMeeking, *International Journal of Solids and Structures* 30 (1990) 1211–1223.
26. G.Th.M. Stam and E. Van der Giessen, *Mechanics of Materials* 21 (1995) 51–71.
27. H.E. Lutz and N. Claussen, *Journal of the European Ceramics Society* 7 (1991) 209–218.
28. H.E. Lutz and N. Claussen, *Journal of the European Ceramics Society* 7 (1991) 219–226.